Title

Critical Assessment of Photoionization Efficiency Measurements for Characterization of Soot-Precursor Species

Journal

The Journal of Physical Chemistry A, 121(23)

ISSN

1089-5639

Authors

Johansson, K Olof

Zádor, Judit

Elvati, Paolo

et al.

Publication Date

2017-06-15

DOI

10.1021/acs.jpca.7b02992

Peer reviewed

Critical Assessment of Photoionization Efficiency Measurements for Characterization of Soot-Precursor Species

K. Olof Johansson,[,1] Judit Zádor,[1] Paolo Elvati,[2] Matthew F. Campbell,[1] Paul E. Schrader,[1] Nicole K. Richards-Henderson,[3] Kevin R. Wilson,[3] Angela Violi,[2,4] and Hope A. Michelsen*[,1]*

[1]Combustion Research Facility, Sandia National Laboratories, Livermore, CA 94550, USA.

[2]Department of Mechanical Engineering, University of Michigan, Ann Arbor, MI 48109, USA.

[3]Chemical Sciences Division, Lawrence Berkeley National Laboratory, Berkeley, CA 94720, USA.

[4]Departments of Chemical Engineering, Macromolecular Science and Engineering, Biophysics Program, University of Michigan, Ann Arbor, MI 48109, USA.

AUTHOR INFORMATION

Corresponding Author

[*]Correspondence and requests for materials should be addressed to H.A.M. (hamiche@sandia.gov) or K.O.J. (okjohan@sandia.gov).

ABSTRACT

We present a critical evaluation of photoionization efficiency (PIE) measurements coupled with aerosol mass spectrometry for the identification of condensed soot-precursor species extracted from a premixed atmospheric-pressure ethylene/oxygen/nitrogen flame. Definitive identification of isomers by any means is complicated by the large number of potential isomers at masses likely to comprise particles at flame temperatures. This problem is compounded using PIE measurements by the similarity in ionization energies and PIE-curve shapes among many of these isomers. Nevertheless, PIE analysis can provide important chemical information. For example, our PIE curves show that neither pyrene nor fluoranthene alone can describe the signal from $C_{16}H_{10}$ isomers and that coronene alone cannot describe the PIE signal from $C_{24}H_{12}$ species. A linear combination of the reference PIE curves for pyrene and fluoranthene yields good agreement with flame-PIE curves measured at 202 u, which is consistent with pyrene and fluoranthene being the two major $C_{16}H_{10}$ isomers in the flame samples, but does not provide definite proof. The suggested ratio between fluoranthene and pyrene depends on the sampling conditions. We calculated the values of the adiabatic-ionization energy (AIE) of twenty-four $C_{16}H_{10}$ isomers. Despite the small number of isomers considered, the calculations show that the differences in AIEs between several of the isomers can be smaller than the average thermal energy at room temperature. The calculations also show that PIE analysis can sometimes be used to separate hydrocarbon species into those that contain mainly aromatic rings and those that contain significant aliphatic content for species sizes investigated in this study. Our calculations suggest an inverse relationship between AIE and the number of aromatic rings. We have demonstrated that further characterization of precursors can be facilitated by measurements that test species volatility.

INTRODUCTION

Soot released from combustion sources is of global concern because it can cause premature deaths,[1] atmospheric hydrological changes,[2-4] and global warming.[5-6] Soot particles released during combustion can be coated with polycyclic aromatic hydrocarbons (PAHs) that are toxic.[7] PAH formation and properties in flames are of great importance, because PAHs are generally considered to be molecular precursors to soot particles.[8-11]

Mass spectrometry is a commonly used method for measuring samples extracted from flames because it enables simultaneous or nearly simultaneous detection of multiple species. In addition to mass analysis, molecular-beam mass spectrometry studies using vacuum ultraviolet (VUV) radiation for photoionization have shown that identification of isomers of small gas-phase hydrocarbons in flames can be accomplished using photoionization-efficiency (PIE) analysis, *i.e.*, analysis of the photon-energy dependence of a peak in a mass spectrum.[12-17] Unambiguous identification of larger isomers, *i.e.*, those containing five or more carbon and oxygen atoms, is challenging,[18] however, because (1) the possible number of isomers grows with the molecular size, (2) isomers of potential importance have small differences in heats of formation (the link between heat of formation and ionization-threshold energy (IE) has been explained and verified for alkanes, alkenes, and monosubstituted alkanes[19]), and (3) similar chemical structures lead to similar IEs and PIE curves.[14] Despite these challenges, PIE measurements have been used to separate isomers of larger species in chemically limited systems, *i.e.*, in systems with a limited number of possible isomers. For example, Zhang *et al*.[20] distinguished indene (C_9H_8) from three of its isomers by comparing experiments and simulated photoionization cross-section curves, and

Parker *et al*.[21] similarly inferred contributions to the signal at 152 u from 2-ethynyl-naphthalene and acenaphthylene ($C_{12}H_8$).

A hydrocarbon flame cannot be considered a chemically limited system *a priori*, and the basis for isomer assignment from PIE measurements needs to be investigated. There are several key areas of investigation related to soot formation during combustion that require measurement techniques capable of delivering chemical information on the molecular level. For example, particle nucleation is critical to soot formation, but is poorly understood. Particle inception is hypothesized to be initiated by large PAHs,[8-11] but the PAH size required for dimerization has not been established. In addition, it is not known if soot-precursor species are predominantly purely aromatic or if they have significant aliphatic content. Soot-formation models use PAH species as small as pyrene as a proxy for soot formation in order to predict soot-particle size distributions.

Pyrene is a stabilomer,[22] *i.e.*, one of the most thermodynamically stable hydrocarbon species, and is considered to be a common $C_{16}H_{10}$ isomer formed during combustion.[23] Schuetz and Frenklach[24] calculated the lifetimes of its dimer at combustion-relevant temperatures and suggested that it survives long enough for subsequent growth and compound stabilization to occur at pressures relevant to, for example, diesel combustion. This result is supported by the study of Herdman and Miller.[25] Elvati and Violi,[26] however, advocated larger species and pointed to the potential importance of aliphatic side chains. Their results are in line with those of Sabbah *et al*.,[27] who measured the pyrene-monomer signal from cold, supersaturated pyrene/buffer gas mixtures and extrapolated their results to conclude that the equilibrium strongly favors pyrene-dimer dissociation at flame temperatures.

In aerosol mass spectrometry studies of soot-precursor species containing more than 10 carbon atoms, the mass peak corresponding to signal from $C_{16}H_{10}$ isomers is generally significant, as are other mass peaks whose masses have stabilomer structures.[28-36] Explicit evidence suggesting the presence or absence of particular isomers is, however, lacking. Some studies have presented results, beyond just molecular masses, that are consistent with the generation of stabilomer species during combustion and pyrolysis of carbonaceous fuels.[37-39] These studies also suggest the presence of several non-stabilomer isomers, for example, fluoranthene, acephenanthrylene, and aceanthrylene at the nominal mass of $C_{16}H_{10}$, *i.e.*, 202 u.[37-39]

The central question for the present work is what kind of information PIE analysis can provide in the study of soot-precursor species, given the challenges described above. Few of the potential soot-precursor species have had their photoionization cross-section curves measured. Pyrene is an exception. Its absolute photoionization cross section has been measured for a wide range of photon energies by Verstraete *et al.,*[40] who discussed the implications of UV photoionization for heating of diffuse interstellar gas. In addition, Li[41] has estimated the photoionization cross-section curve between the IE of 7.43 eV and 11.77 eV, and we have derived the photoionization cross-section curve between 7.5 and 10.2 eV in a companion paper.[42] Pyrene's relative photoionization cross-section curve has been measured by Tobita *et al*.[43] and Johansson *et al*.[32] Relative PIE-curve shapes are sufficient for identifying isomers without quantifying the relative concentrations, provided that the PIE-curve shapes of the different isomers are dissimilar enough to allow separation. The pyrene photoionization cross section measured by Verstraete *et al.*[40] and Johansson *et al.*[32] were recently used to prove that $C_{16}H_{10}$ isomers other than pyrene were detected among soot-precursor species extracted from ethylene flames.[32] In addition, we have

previously compared the PIE curve from a soot sample sampled from an acetylene counter-flow flame to Li's[41] estimated photoionization cross-section curve.[31]

In this work, we have evaluated the insight provided by PIE measurements performed on samples collected from a premixed ethylene flame. The results show that quantitative isomer speciation is impossible, or nearly so. Nevertheless, we demonstrate that PIE analysis can provide insight into soot-formation chemistry and can sometimes be used to partition precursor-species distributions into two classes of species, one class of species that contain several aromatics rings and another class of species that are purely aliphatic or contain only a few aromatic rings. We also demonstrate that PIE analysis can provide additional insight by indicating a need to include new isomers in soot-formation models. We have used quantum chemistry to calculate the values of the adiabatic-ionization energy (AIE) of twenty-four $C_{16}H_{10}$ isomers. These calculations confirm that the differences in AIEs between different isomers can be smaller than the average thermal energy at room temperature, even for a relatively small subset of isomers. We also show that neither pyrene nor fluoranthene alone can account for the PIE signals from $C_{16}H_{10}$ isomers in the present flame, even though a reasonable match for the flame-measured curves of $C_{16}H_{10}$ isomers can be found by considering a combination of pyrene and fluoranthene signals. We similarly demonstrate that coronene alone cannot account for the PIE signal from $C_{24}H_{12}$ isomers. We furthermore show that measurements that provide information about species volatility can be used with PIE analysis to facilitate characterization of precursor species.

EXPERIMENTAL SECTION

Beamline and Instrument

Measurements were performed at the Chemical Dynamics Beamline at the Advanced Light Source at Lawrence Berkeley National Laboratory in Berkeley, CA, USA. The instrument used was an aerosol mass spectrometer. It consists of three pumping stages, and the sample is injected *via* an aerodynamic lens system (ADL).[44-46] The pressure behind the inlet nozzle feeding the ADL is about 1 to 2 Torr. The outlet of the ADL is in the first stage vacuum chamber (4.5 inch spherical cube from Kimball Physics). The ADL acts as a filter against gas-phase molecules and small particles; it focuses particles larger than ~50 nm into a beam while small particles and gas-phase molecules follow Brownian motion and are pumped away by the turbo-molecular vacuum pumps.[45-46] Thus, gas-phase PAHs have to condense onto existing particles that are either larger than, or that grow to, ~50 nm in the sampling line in order to be efficiently detected by the aerosol mass spectrometer, and the strong suppression of light gas-phase species using this instrument has been revealed in previous studies.[30-32, 47] Because detected species are in a condensed phase at ambient conditions and are vaporized from soot particles in the ionization region, we refer to the mass spectra as aerosol mass spectra.

The second vacuum chamber (4.5-inch spherical cube from Kimball Physics) acts as a differential pumping stage. The third chamber is the ionization chamber (custom 10-inch diameter cylindrical vessel with multiple conflat ports), and it has an operating pressure of ~7×10^{-7} Torr. The particles focused by the ADL impinge on a target copper plate, which is heated to ~300 ˚C and is located near the center of the ionization chamber. After striking the target, species that are weakly bound to the particles are vaporized. The relatively low temperature of the aerosol target restricts fragmentation but may limit the signal from high-mass

species. A quasi-continuous beam of tunable vacuum-ultraviolet (VUV) radiation from the synchrotron passes ~1.9 mm in front of the aerosol target and is used for single-photon ionization of vaporized species. The resulting ions are pulse extracted into a time-of-flight mass spectrometer at a rate of 15 kHz. We assume singly ionized species and henceforth refer to the nominal molecular mass in unified mass units (u) instead of the mass-to-charge ratio.

A 30-torr Ar gas filter and a magnesium fluoride (MgF_2) window was used in the beam path to prevent high harmonics of the synchrotron radiation from entering the ionization region of the mass spectrometer. The resulting photon-energy distribution was relatively broad (~0.2 eV full-width at half-maximum). In addition, the photon-energy distribution was delivered with a relatively spectrally broad background of low photon flux.

Flame Measurements

Particles were sampled from a premixed flame operated at atmospheric pressure. We used a McKenna-type burner with a 38.1-mm brass-porous plug surrounded by an outer shroud-gas porous-plug ring and a stabilization plate located 13.3 mm above the porous plug. The gas-flow rate through the central porous plug was a mixture of 0.67 slm (standard liters per minute referenced to 0 ˚C and 101325 Pa) C_2H_4, 0.96 slm O_2, and 3.62 slm N_2. The shroud-gas flow rate through the outer ring was 19 slm N_2. The temperature profile of this flame has been measured using coherent Raman imaging, and the maximum temperature is similar to those measured in ethylene McKenna flames with similar equivalence ratios, but larger burner-to-stabilization plate distance.[48]

Soot particles and gas-phase flame species were sampled along the vertical centerline of the flame using a horizontally positioned quartz probe. This probe had been manufactured from a straight quartz tube with an OD of 3 mm and an ID of 2 mm. The last ~5 mm of the probe end facing the flame was tapered down to a tip opening of ~400 μm, and the probe extracted sample from the flame at a rate of ~0.100 slm. The relatively large opening diameter of the probe tip was necessary in order to avoid clogging of the probe by soot particles during the measurements. The quartz probe was connected to an aluminum probe block that was normally heated to ~80 ˚C. The probe block is ~25 mm long, and the ID of the sample channel inside the block is ~8.5 mm. The probe block was connected to a ~50-cm long, 6.35-mm OD, 4.57-mm ID copper tube that was connected to the inlet nozzle of the ADL on the aerosol mass spectrometer. The total residence time in the sampling system leading to the ADL was ~8 s, and the sample gas and particles were never exposed to atmospheric oxygen.

A 38.1 cm long diffusion dryer (Droplet Measurement Technologies) and a thermal denuder were in place between the quartz probe and the ADL during some of the measurements. The thermal denuder is based on the design of Fierz *et al*.,[49] and it was used to remove the most volatile species that condensed onto the soot particles in the probe and in the sampling line. It consists of three equal-length heated sections with separate heaters. The walls surrounding the full length of the inner flow tube (30 cm long, 9.5 mm diameter) contain activated charcoal that traps volatile species. The hottest section was heated to 175 ˚C.

Quantum Chemistry Calculations

We calculated the AIEs of twenty-four $C_{16}H_{10}$ isomers using density functional theory (DFT) with the M06-2X functional in combination with the 6-31+G(d,p) and the 6-311++G(d,p) basis sets and the CBS-QB3 quantum composite method as implemented in the Gaussian 09 program package.[50] We included zero-point energy corrections, but did not consider the effect of Franck-Condon overlaps,[14, 51] which, in the case of poor origin band overlaps between the neutral and the cation, can shift the experimental appearance threshold higher, or, in the case of hot bands, can lower it. We started the cation calculations from the same conformer geometries as those of the neutrals. This way we assumed that cations with significantly different geometries from the neutral species have very little Franck-Condon overlap, even if these cation geometries represent the global minima on the cation potential energy surfaces. We also confirmed that the ground states of all isomers are singlets (rather than triplets) at the M06-2X/6-31+G(d,p) level of theory.

RESULTS AND DISCUSSION

The signal from $C_{16}H_{10}$ (202 u) isomers obtained from soot samples is often substantial, as demonstrated in several previous studies.[28-36] Figure 1a and c show aerosol mass spectra of soot extracted from the premixed flame at a height above the burner (HAB) of 6 and 10 mm, respectively. The sampling line used for extraction of the samples yielding the signals presented in Fig. 1 was heated to ~80 ˚C. The signals at 202 u and other light masses were even stronger in the spectra recorded without the thermal denuder when the sampling line was kept at room temperature. This result suggests that, in the absence of heating, there is significant condensation of light species onto existing particles in the sampling line.

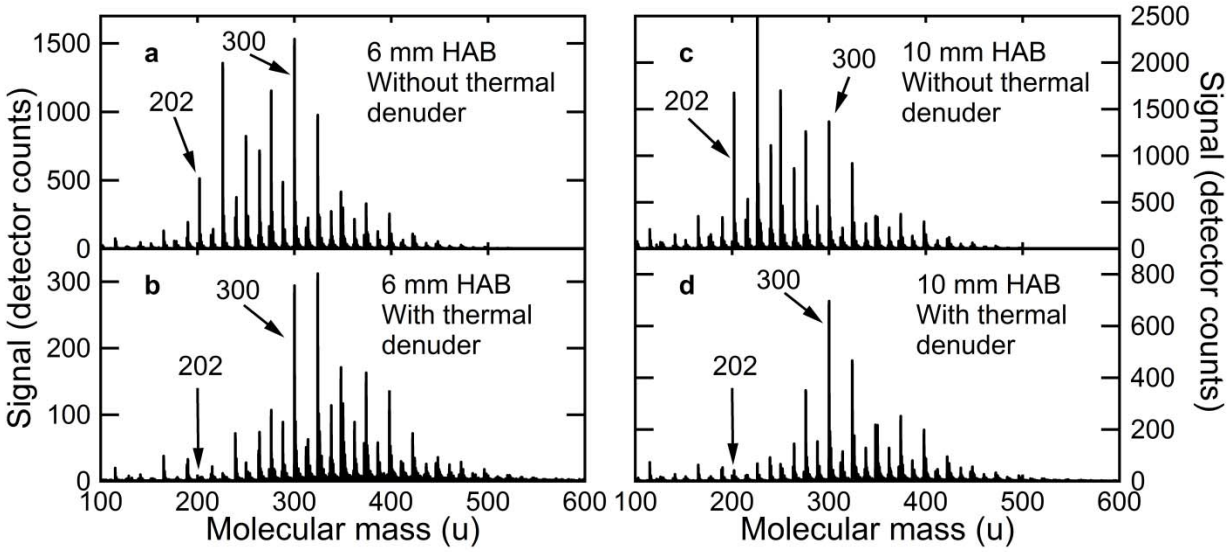

Fig. 1. Aerosol mass spectra recorded in the premixed ethylene/oxygen/nitrogen flame: Mass spectra were recorded at 6 mm (a) without and (b) with a thermal denuder in front of the mass spectrometer and at 10 mm (c) with and (d) without the thermal denuder. Mass peaks at 202 ($C_{16}H_{10}$ isomers) and 300 u ($C_{24}H_{12}$ isomers) are indicated.

The PIE curves recorded at 202 u at 6 and 10 mm HAB are plotted in Fig. 2. In a companion paper we report the PIE curves of the two $C_{16}H_{10}$ isomers pyrene and fluoranthene.[42] The PIE curves of these two species were measured using the present aerosol mass spectrometer at the same beamline end station as used to measure the flame samples and during the same beamtime cycle. Figure 2a shows the pyrene-PIE curve, and Fig. 2b shows the fluoranthene-PIE curve. None of the curves shown in Fig. 2 have been corrected for the background or the photon flux differences at different photon energies. The error bars represent 95% confidence intervals of the standard errors of the mean of 13 scans for pyrene, 12 scans for fluoranthene, 3 scans for the flame samples extracted at an HAB of 10 mm, and 2 scans for the flame samples extracted at an HAB of 6 mm. The upper and lower confidence-interval limits for each curve were calculated as

$\bar{x} \pm 1.96\sigma/\sqrt{n}$, where $\bar{x}$ is the mean value, σ is the standard deviation, and n is the number of sampled curves. The flame-PIE curves in Fig. 2a have been fit to the pyrene-PIE curve in the photon-energy range 8.5-9.5 eV using a scaling factor and an offset component. This fitting gives overlap with the pyrene curve in the energy range 8.5-9.5 eV but results in low values of the flame-PIE curves relative to the pyrene curve below 8.5 eV. The original flame-PIE curves did not have zero signal levels at 7.5 eV. The offset subtraction and scaling were performed in order to compare the curve shapes of the flame-PIE curves to that of pyrene, and the y-values attained are not quantitative. The offsets obtained from the fits should not be confused for actual signal backgrounds, because the offsets lack physical meaning unless only pyrene contributes to the flame-PIE signals.

Similar fits were performed to the fluoranthene-PIE curve shown in Fig. 2b. The results of these fits using the same flame-PIE curves are also shown in Fig. 2b. In this case, the flame-PIE curves are higher than that of fluoranthene below 8.5 eV. In addition, at energies between 9.5 and 10 eV, the flame-PIE curves lie slightly above the pyrene curve in Fig. 2a while they lie slightly below the fluoranthene curve in Fig. 2b.

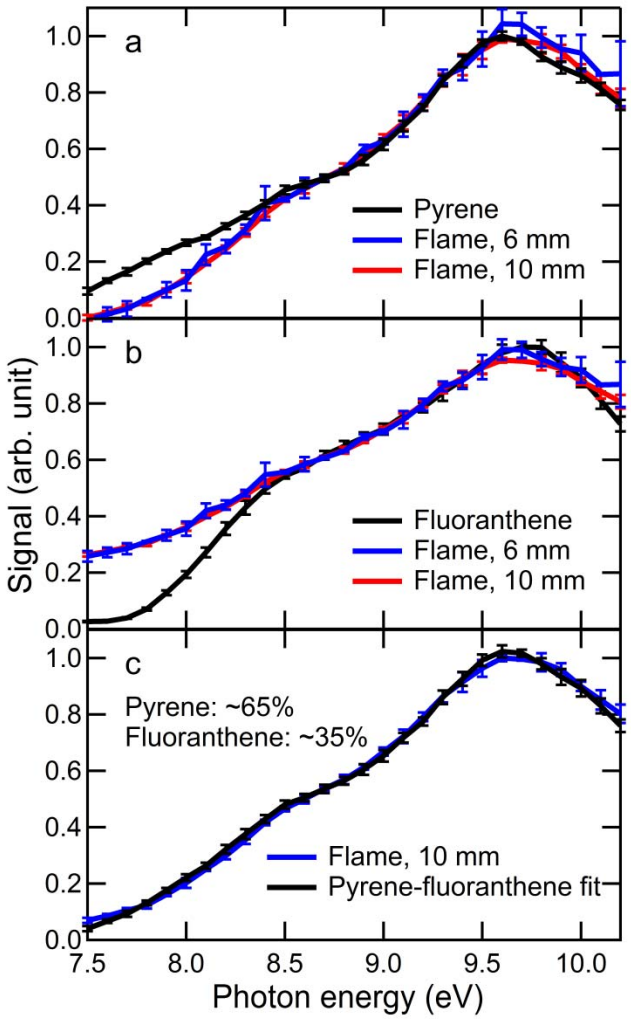

Fig. 2. Comparison of flame PIE and known PAH-PIE curves for mass 202 u. Flame samples were extracted from a premixed ethylene/oxygen/nitrogen flame at HABs of 6 and 10 mm. (a) Comparison between the shapes of the pyrene-PIE curve and the flame-PIE curves of soot samples drawn from the flame. The flame-PIE curves were scaled and offset to fit the pyrene-PIE curve between 8.5 and 9.5 eV (see text for details). (b) Same as in (a), but with the flame-PIE curves fit to the fluoranthene-PIE curve. (c) Comparison between the flame-PIE curve recorded from samples drawn at an HAB of 10 mm and the best fit of the PAH curves to the flame curve using a linear combination of the pyrene- and fluoranthene-PIE curves.

The two flame-PIE curves in Fig. 2 are nearly identical throughout the entire photon-energy range, suggesting that the $C_{16}H_{10}$ isomeric compositions are similar at the two HABs. Neither the pyrene-PIE curve nor the fluoranthene-PIE curve can describe the flame-PIE curves. This result is consistent with previous results with respect to pyrene.[31-32] Figure 2c shows a two-component fit using the pyrene and fluoranthene-PIE curves as basis functions. The fit is a linear combination of the pyrene- and fluoranthene-PIE curves fit to the flame-PIE curve at 10 mm. The fit suggests that pyrene contributes ~65% of the signal and fluoranthene ~35%. A similar fit to the flame-PIE curve at 6 mm suggested ~70% pyrene and ~30% fluoranthene. The speciation suggestions obtained from the fits at the two HABs were expected to be similar because of the similarities between the two flame-PIE curves. The small differences in fit results for the speciation are statistically insignificant considering the relatively low averaging of the flame-PIE curves.

The composite pyrene-fluoranthene curve and the flame-PIE curve in Fig. 2c are nearly identical throughout the entire photon-energy range. This result is consistent with pyrolysis studies[38-39] and studies on soot samples from inverse diffusion flames,[37] which have suggested significant contributions from both pyrene and fluoranthene. Despite the agreement between the fit and the flame data, the resulting speciation is far from conclusive. There is a large number of isomers of $C_{16}H_{10}$ that could contribute to the flame signal at this mass, and many of them have similar structures and likely similar PIE curves. Thus, the PIE curves of all possible isomers cannot be expected to constitute a linearly independent basis set for fitting to the data. We have, in the present analysis, only considered the reference PIE curves of two species and these two (pyrene and fluoranthene) have very dissimilar PIE curves.

Furthermore, PIE analysis requires extractive sampling, and detected species are influenced by perturbations to the chemical composition caused by the probe and transport in the sampling line. Insufficiently rapid quenching of the chemistry during sampling could lead to consumption of some species and condensation of others, thereby yielding a perturbed species distribution relative to the original distribution in the flame. The measured particle composition is also not likely to replicate the gas-phase composition in the flame, despite condensation of semi-volatile species as the particles are cooled in the probe. Sampling may lead to a bias for the least volatile gas-phase isomers.

In order for a species to be efficiently detected by the aerosol mass spectrometer, the species must either be in the particle in the flame or condense onto particles near the probe or inside the probe and sampling line and remain condensed all the way to the ionization region where it vaporizes. Molecules that do not condense and thus enter the ADL in the gas phase will not be focused by the ADL and are therefore unlikely to make it to the ionization region. The temperature of the sampling line therefore affects the measured speciation, as confirmed by our flame-PIE curves at 202 u; curves recorded with the sampling line at room temperature had a different shape than the PIE curves recorded with the sampling line heated to ~80 ˚C. This result proves that more than one isomer contributed to the observed signal at 202 u and at least two of the contributing isomers have different volatilities. Signal loss due to heating of the sampling line would be found by directly observing the mass-peak intensity with and without heating, but to prove the contribution from more than one isomer requires PIE-curve comparison.

Fluoranthene melts and boils at lower temperatures than pyrene and is more volatile. The two-component fit to the signal recorded with the cold sampling line suggested that fluoranthene contributed more to the 202-u signal than pyrene, but pyrene contributed more than fluoranthene

to the signal when the sampling line was heated. Hence, the inferred isomer fractional contributions from the two-component pyrene-fluoranthene fits were consistent with fluoranthene being more volatile than pyrene, and provide support for the result suggested by the fit in Fig. 2c that pyrene and fluoranthene may be important signal contributors at 202 u.

Calculations of the Adiabatic Ionization Energies of Twenty-Four $C_{16}H_{10}$ Isomers

The shape of a PIE curve is determined by the overlap between the vibrational wavefunctions of the neutral molecule and the cation. The simplest property of these curves is their onset identified by the AIE, which is an important parameter to consider when assessing isomer discrimination based on PIE analysis. If measurements are not available, AIEs can be calculated using quantum chemistry. We performed AIE calculations for $C_{16}H_{10}$ isomers (Table 1) to gain insight into the IE differences that can be expected between large hydrocarbon isomers. The number of isomers is large, in excess of 964, which is the number of conjugated tetracyclic $C_{16}H_{10}$ isomers containing all 16 carbon atoms distributed among the 4 rings.[52] We included a subset of twenty-four isomers in our calculations, and five of these have purely conjugated tetracyclic structures. The twenty-four isomers are shown in Fig. 3. Several of these isomers are predicted to be among the $C_{16}H_{10}$ species generated in combustion,[31, 47, 53-54] and for some of them there is experimental evidence suggesting their formation during combustion and pyrolysis.[37-39]

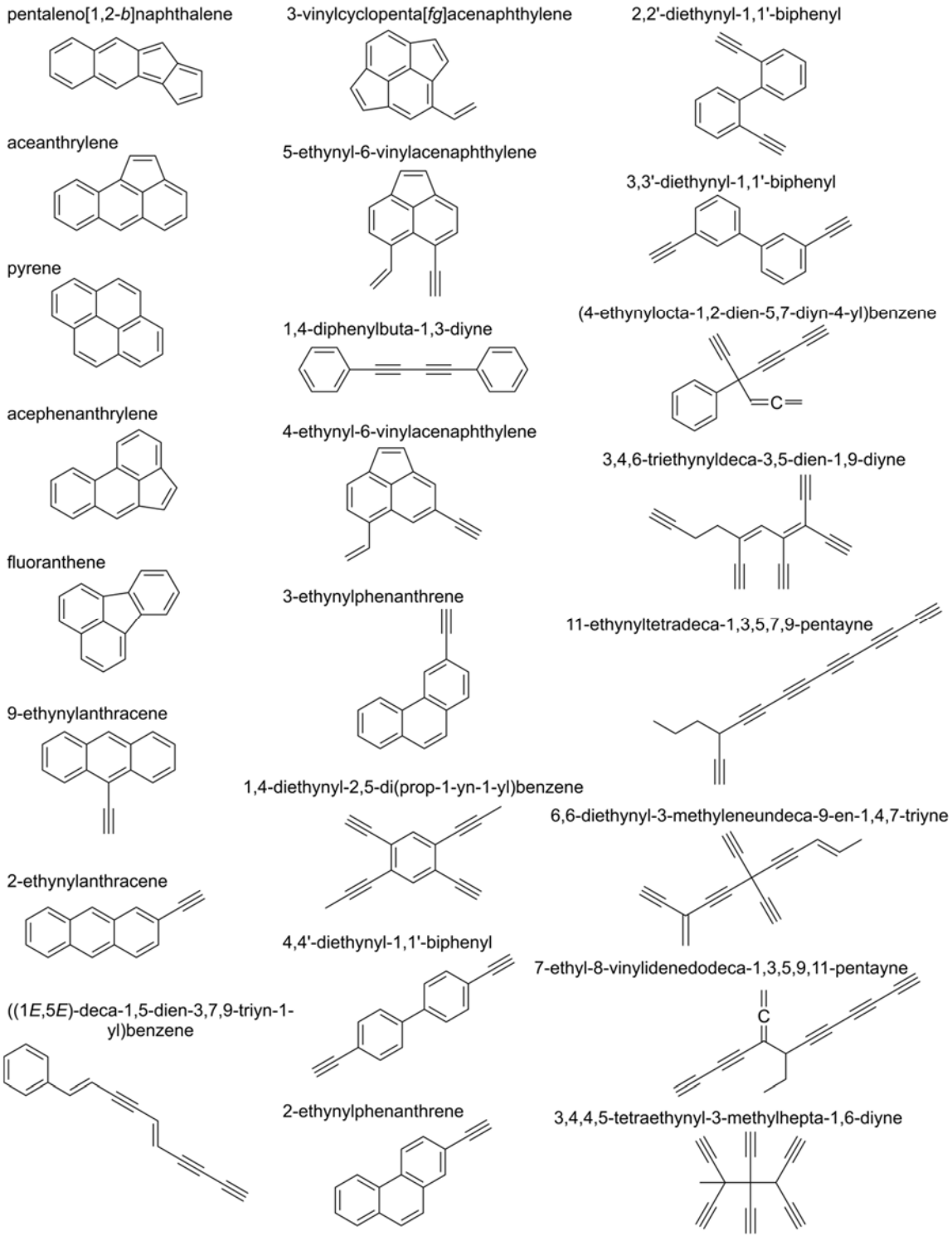

Fig. 3. $C_{16}H_{10}$ isomers studied using quantum chemistry calculations.

The open-shell cations suffered from very large spin contaminations in the CBS-QB3 calculations, where the eigenvalue of the spin operator ($<S^2>$) was as high as 5.6 instead of the theoretical value ($<S^2_{th}>$) of 0.75. (The calculations did not converge for 11-ethynyltetradeca-1,3,5,7,9-pentayne). The AIEs calculated using CBS-QB3 are likely to be too high because of significant mixing of higher energy-spin states into the cation wavefunctions, although the method includes a correction term for this mixing, $\Delta E_{spin} = -0.00954\ E_h\ (<S^2> - <S^2_{th}>)$, where $E_h = 27.2114$ eV converts Hartree to eV. The correction term, ΔE_{spin}, is more than 1 eV for $<S^2> = 5.6$, and the CBS-QB3 results potentially have an unusually large uncertainty. Nevertheless, the agreement with the DFT calculations is satisfactory, except for 3-vinylcyclopenta[fg]acenaphthylene, which has the highest spin contamination amongst the species in the cation state for which the CBS-QB3 calculations converged as shown in Table 1. The DFT calculations themselves did not have spin contamination problems and showed good agreement across the two basis sets. We also ran ROCBS-QB3 calculations, which, by definition, have no spin contamination but did have convergence issues.

In order to further understand the uncertainties of our calculations, we compared the calculated AIEs with experimentally measured IEs for those isomers that have values readily available in the literature. These compounds are pyrene, fluoranthene, 1,4-diphenylbuta-1,3-diyne, and 2,2'-diethynyl-1,1'-biphenyl. The difference between any of the calculated and the experimental values is ≤0.1 eV for all four molecules, despite the fact that the latter two species suffered from large spin-contamination effects in the CBS-QB3 calculations (see Table 1).

Table 1. Adiabatic ionization energies for selected $C_{16}H_{10}$ isomers. See text for more details.

$C_{16}H_{10}$ isomer*	AIE (eV)	$<S^2>$	IE (eV)

	M06-2X/ 6-31+G(d,p)	M06-2X/ 6-311++G(d,p)	CBS-QB3	CBS-QB3	Literature
Only conjugated rings					
pentaleno[1,2-b]naphthalene	7.28	7.33	7.40	2.1935	
aceanthrylene	7.37	7.42	7.53	2.2300	
pyrene	7.39	7.43	7.47	0.9769	7.43[55]
acephenanthrylene	7.79	7.84	7.96	4.1257	
fluoranthene	7.86	7.90	7.91	0.8082	7.90[56]
Aliphatic side chain(s) or bridge					
9-ethynylanthracene	7.30	7.35	7.35	0.842	
2-ethynylanthracene	7.38	7.43	7.51	1.3716	
((1E,5E)-deca-1,5-dien-3,7,9-triyn-1-yl)benzene	7.42	7.48	7.59	4.8859	
3-vinylcyclopenta[fg]acenaphthylene	7.44	7.49	6.68**	5.6564	
5-ethynyl-6-vinylacenaphthylene	7.68	7.73	7.93	2.6904	
1,4-diphenylbuta-1,3-diyne	7.70	7.75	7.89	2.3725	7.8,[57] 7.9[58]
4-ethynyl-6-vinylacenaphthylene	7.76	7.80	7.87	3.9015	
3-ethynylphenanthrene	7.79	7.83	7.90	1.7548	
1,4-diethynyl-2,5-di(prop-1-yn-1-yl)benzene	7.79	7.84	7.91	1.0772	
4,4'-diethynyl-1,1'-biphenyl	7.93	7.99	7.98	2.5063	
2-ethynylphenanthrene	7.94	7.97	8.01	1.7961	
2,2'-diethynyl-1,1'-biphenyl	8.18	8.23	8.24	2.8474	8.20[59]
3,3'-diethynyl-1,1'-biphenyl	8.25	8.29	8.35	2.8064	
(4-ethynylocta-1,2-dien-5,7-diyn-4-yl)benzene	8.53	8.54	8.70	1.7162	
Purely aliphatic					
3,4,6-triethynyldeca-3,5-dien-1,9-diyne	7.66	7.72	7.79	1.6088	
11-ethynyltetradeca-1,3,5,7,9-pentayne	8.21	8.33	-	5.9372	
6,6-diethynyl-3-methyleneundeca-9-en-1,4,7-triyne	8.24	8.30	8.54	1.3008	
7-ethyl-8-vinylidenedodeca-1,3,5,9,11-pentayne	8.36	8.43	8.62	1.2054	
3,4,4,5-tetraethynyl-3-methylhepta-1,6-diyne	8.90	8.96	9.13	0.7525	

*Structures for these species are shown in Fig. 3.

**This value is likely to be incorrect because of the large spin contamination.

All twenty-four isomers included in the study have calculated AIEs falling within a range of ~1.6 eV, and several of the isomers are predicted to have AIEs that differ from each other by less than the average thermal energy at room temperature (0.03 eV), *e.g.*, pyrene, aceanthrylene, and 2-ethynylanthracene at ~7.43 eV and acephenanthrylene, 3-ethynylphenanthrene, and 1,4-

diethynyl-2,5-di(prop-1-yn-1-yl)benzene at ~7.84 eV (M06-2X/6-311++G(d,p)). Narrow spreads in IEs are expected for hydrocarbon species containing many carbon atoms,[14] which makes isomeric identification based on measured ionization thresholds difficult. In addition, the uncertainties in the AIE calculations are larger than the differences in AIE between many of the listed isomers. For these large species, however, significantly more accurate calculations are unfeasible.

For many systems the number of potentially important isomers may be reduced based on, for example, formation-energy barriers, thermal decomposition, and reaction pathways. The number of potentially important isomers is expected to grow with molecular size, and the overall differences in IEs are expected to become smaller.[14] Therefore, some *a priori* knowledge about the system would most likely be necessary in order to reduce the number of isomers that need consideration. If theoretical considerations and flame-chemistry modeling can reduce the number of potentially important isomers to a handful, PIE analysis is much more likely to prevail in providing reliable isomer identification and quantification.

Nevertheless, PIE analysis can be helpful even in the absence of *a priori* information that reduces the number of potential isomers. Table 1 is organized in three groups, *i.e.*, species containing only conjugated rings, species that have both conjugated rings and aliphatic structures, and fully aliphatic species. Furthermore, the species in each group are organized in ascending order with respect to their calculated AIE values. Table 1 shows that there is a significant AIE overlap among species with different aromatic and aliphatic content. Nevertheless, AIE values at and above 8 eV are found only among species in the third group and in the lower section of the second group. Hence, a measured IE value larger than 8 eV suggests that the detected species contain aliphatic structures or are fully aliphatic. However, a thorough

and efficient investigation of the structure and size dependence of the AIEs is likely best done through empirical correlations using scaled HOMO energies.[60]

Figure 4 shows a comparison of PIE curves for 200 u and 202 u from sample extracted at an HAB of 10 mm. The 202-u PIE curve is reproduced from Fig. 2, but has only been normalized whereas the curves in Fig. 2 were scaled and offset to fit the PIE curves of pyrene (Fig. 2a) and fluoranthene (Fig. 2b). The 200-u curve was extracted from the same mass spectra as the 202-u curve and is an average of three individual PIE measurements. The flatness of the PIE curve for 200 u in Fig. 4 below ~7.9 eV suggests that the non-zero signal level at the lowest photon energies is due to background. The IE value appears to be ~7.9 eV, but the actual threshold would have appeared near 8.1 eV if the photon-energy distribution had been narrower and had not contained a spectrally wide background of low photon flux. Hence, assuming similar IE values for similarly structured species weighing 200 and 202 u, the signal at 200 u is likely to stem predominantly from molecules with significant aliphatic content. The apparent difference in IE between the flame-PIE curves at 200 and 202 u can possibly be explained by the difference in hydrogen content. The H/C of $C_{16}H_{10}$ (202 u) can support perfectly sp^2-hybridized aromatic structures, but the structures of $C_{16}H_8$ and $C_{15}H_{20}$ (200 u) yield aliphatic content.

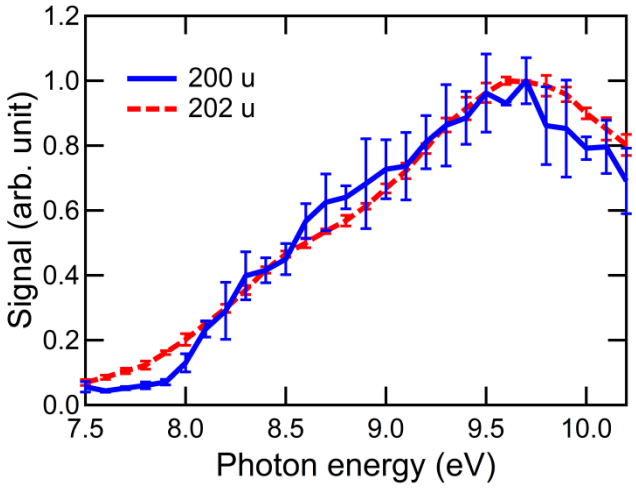

Fig. 4. Average PIE curves of the signals at 200 u and 202 u from soot samples extracted from the atmospheric premixed ethylene/oxygen/nitrogen flame at an HAB of 10 mm. The averaged curves have not been corrected for either the background or the photon-flux differences at different photon energies, and the error bars represent 95% confidence intervals of the standard errors of the mean.

We can rule out the $C_{16}H_8$ stabilomer species (3-ethynylcyclopenta[fg]acenaphthylene) from being a signal contributor at 200 u because its calculated AIE (M06-2X/6-311++G**) is 7.62 eV, *i.e.*, ~0.5 eV from the actual IE of ~8.1 eV at 200 u. This result has chemical implications; Parker *et al.*[21] showed that acetylene addition to naphthyl radicals in a high-temperature reactor led to formation of acenaphthylene, ethynylnaphthalene, and diethynylnaphthalene, but not anthracene or phenanthrene.[21] Their experimental results are in agreement with the theoretical study performed by Kislov *et al.*,[61] which showed that the HACA mechanism[23, 62] preferentially leads to formation of five-membered rings in the molecular growth beyond naphthalene during combustion. In addition, the 3-ethynylcyclopenta[fg]acenaphthylene stabilomer species was recently predicted by a HACA-dominated mechanism to be among the most commonly produced

soot-precursor species containing 16 carbon atoms in an acetylene counter-flow flame.[31] Thus, the HACA mechanism would be expected to yield the $C_{16}H_8$ stabilomer 3-ethynylcyclopenta[fg]acenaphthylene at 200 u. The absence of detectable signal from this species suggests that alternative chemical growth pathways to the HACA mechanism are important in the present flame. The absence of the $C_{16}H_8$ stabilomer species is unlikely to be attributable to probe and sampling perturbations as this species is the most thermodynamically stable molecule at this mass and therefore unlikely to change its structure in and around the microprobe. In addition, the sample was extracted from a high flame height (10 mm HAB), which minimizes probe perturbations on the growth chemistry that takes place lower in the flame. This example shows how PIE and IE analysis can sometimes provide information on chemical pathways.

Flame Measurements Using a Thermal Denuder

A thermal denuder with the hottest section heated to a temperature of ~175 ˚C (close to atmospheric pressure) was installed in front of the inlet nozzle to the aerosol mass spectrometer in order to better understand the impact of gas-phase condensation in the sampling line. A thermal denuder removes volatile particle coatings by vaporizing species from particle surfaces. Vaporized hydrocarbon species are then trapped by activated carbon along the inner walls of the thermal denuder. Typical aerosol mass spectra recorded with the thermal denuder in place are shown for HABs of 6 mm in Fig. 1b and 10 mm in Fig. 1d. The mass-peak distributions are shifted to higher masses compared to the corresponding mass spectra recorded without the thermal denuder in place (Fig. 1a and c).

The thermal denuder eliminated a significant fraction of the total signal measured by the aerosol mass spectrometer, but the signal was preferentially removed at low masses. At 202 u, for example, almost all the signal was removed. Hence, the signal at 202 u is likely entirely attributable to species that had condensed onto soot particles in the probe and in the sampling line where the temperature was lower than in the flame. Thus, the 202-u species are not likely to condense onto particles at typical flame temperatures of ~1700 K where soot is formed, because they are readily vaporized by the relatively low temperature of the thermal denuder. Nevertheless, these lighter species can still be important for the molecular growth leading to the species that eventually nucleate and condense onto existing soot particles in the flame.

Figure 1 shows that the mass peaks at and above 300 u were less affected by the thermal denuder than the majority of the peaks at lower masses. The relatively strong signals at 300 u with and without the thermal denuder in place allow the PIE curves to be compared. Figure 5 shows a comparison between flame-PIE curves at 300 u recorded with and without the thermal denuder in place. The sampling line was always heated to ~80 ˚C. The coronene-PIE curve presented in our companion paper[42] is also shown in Fig. 5. The flame-PIE curves recorded without the thermal denuder are averages of two (6 mm) and three (10 mm) recordings. The curve recorded at 6 mm HAB with the thermal denuder in place is the average of 3 scans, and 19 scans were averaged to yield the coronene curve. The curves recorded with and without the thermal denuder at an HAB of 6 mm are nearly identical throughout the entire photon-energy range. In addition, these error bars overlap the error bars of the PIE curve recorded at an HAB of 10 mm at most photon energies.

The three flame-PIE curves in Fig. 5 have been fit to the coronene curve between 8.5 eV and 9.5 eV in the same manner as the flame-PIE curves at 202 u were fit to the pyrene and

fluoranthene-PIE curves in Fig. 2a and b. Figure 5 shows that the three flame-PIE curves deviate substantially from the coronene-PIE curve at low photon energies. Thus, the coronene-PIE curve alone cannot account for the flame-PIE signals, and $C_{24}H_{12}$ isomers other than coronene have to be considered to gain a better understanding of the soot-precursor chemistry under these conditions. In addition, the flame-PIE curves suggest that, if the signal-contributing isomers have PIE curves that are distinguishable at the present resolution, the measured speciation is similar at the two HABs and unaffected by the use of the thermal denuder. This result is consistent with larger species near 300 u being less volatile than the lighter species near 202 u.

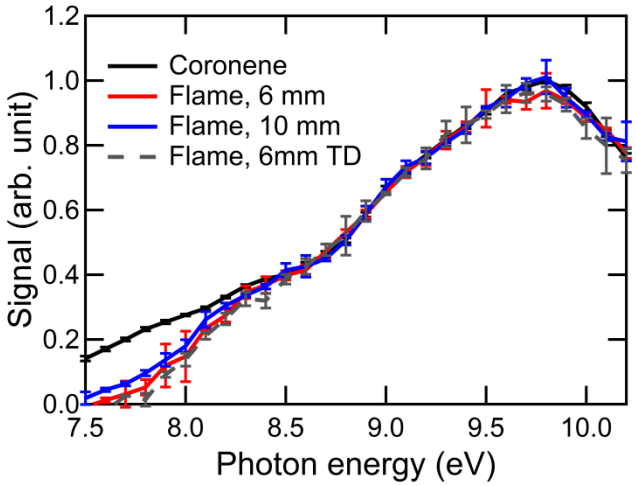

Fig. 5. Comparison between the PIE curve of pure coronene and the flame-PIE curves at 300 u (samples extracted at HABs of 6 and 10 mm). A thermal denuder was in position during the recording of the dashed curve. The raw flame-PIE curves did not have zero signal levels at 7.5 eV, and the low curve values at low photon energies resulted from fits to the coronene-PIE curve (see text related to the fitting of the flame-PIE curves at 202 u to the pyrene-PIE curve for details). The error bars are 95% confidence intervals of the standard errors of the mean.

Direct quantification of the impact of the thermal denuder by restricting the analysis to mass-peak intensities might not lead to the same conclusion as that provided by including PIE analysis. The reason is that the thermal denuder can affect the signal in several ways. There could be a direct loss of particles in the thermal denuder, which causes an overall loss of signal at all masses. Furthermore, as already mentioned and shown by Fig. 1, the thermal denuder removed volatile hydrocarbon species, for example the $C_{16}H_{10}$ isomers, from the particles, which ought to have influenced the signal in two ways. First, molecules trapped by the thermal denuder could obviously not be detected by the aerosol mass spectrometer. Second, removal of volatile coatings from the particles leads to a reduced average particle size. A size reduction likely results in a less tightly focused particle beam exiting the ADL. A more diverging particle beam would reduce the rate at which particles reached the ionization region and would also yield a signal reduction for heavier species. Hence, direct analysis of the mass-peak intensities recorded with and without the thermal denuder in place may lead to incorrect conclusions. For example, the mass-peak intensity at 300 u is significantly lower in Fig. 1b and d than in Fig. 1a and c, which may be interpreted as a selective loss of only the most volatile $C_{24}H_{12}$ isomers in the thermal denuder. This interpretation, however, is not supported by the PIE analysis in Fig. 5, which shows that the PIE-curve shape does not change when the thermal denuder is used. Nevertheless, as neither of the analyses is conclusive, additional studies would be required to draw a firm conclusion.

SUMMARY AND CONCLUSIONS

We have shown that PIE analysis of heavy hydrocarbon species formed in hydrocarbon combustion has severe limitations that cannot easily be overcome. The large number of potential isomers at large masses associated with soot particles makes particle speciation extremely difficult. For PIE analysis, the problem is exacerbated by the similarity in ionization energies and PIE-curve shapes. Nevertheless, we have also shown that PIE analysis of heavy hydrocarbon species can provide important information about soot-precursor chemistry. Information obtained from PIE measurements can sometimes yield new insight and alter conclusions drawn from mass spectra recorded at one fixed photon energy.

Because two isomers with distinguishable IEs can be discriminated by their PIE curves, the limitations of PIE analysis are partly exemplified by the present calculations of AIEs for twenty-four $C_{16}H_{10}$ isomers. Despite the small number of isomers considered, the calculations show that the differences in AIE between several of the isomers are less than the average thermal energy at room temperature. Thus, theoretical input that limits the number of potential isomers to a handful can change the outcome of PIE analysis and may enable quantitative isomer separations of heavy hydrocarbon species.

PIE analysis can provide ample information about particle speciation, despite its quantitative shortcomings. For example, we have shown that neither pyrene nor fluoranthene alone can describe the signal from $C_{16}H_{10}$ isomers on particles extracted from a premixed ethylene/oxygen/nitrogen flame at atmospheric pressure. A linear combination of the reference PIE curves for pyrene and fluoranthene, however, yields good agreement with PIE curves measured at 202 u from the flame-particle samples. Hence, the PIE analysis is consistent with pyrene and fluoranthene being the two major $C_{16}H_{10}$ isomers in the flame-particle samples, but

does not provide definitive proof. The suggested ratio between fluoranthene and pyrene depends on the sampling conditions.

Similarly, the PIE curves at 300 u from the flame-particle samples showed that coronene alone cannot explain the shape of the signal. Thus, stabilomer species alone cannot account for the heavy hydrocarbon species that comprise the particles. The limitations of the stabilomer grid are bolstered by the fact that extractive sampling is likely to preferentially lead to detection of the most stable species, *i.e.*, the stabilomers. Yet, the flame-PIE curves show that isomers other than stabilomers are necessarily present in the samples. Therefore, we have shown that PIE analysis can partly rule out conclusions drawn based on the observed sequence of strong peaks in a mass spectrum recorded at a fixed energy. Similarly, PIE analysis can provide important information related to changes in mass-peak intensities obtained during different sampling conditions.

The AIE calculations performed for twenty-four $C_{16}H_{10}$ isomers show that PIE analysis can sometimes be used to separate heavy hydrocarbon species into those that are predominantly aromatic and those that have significant aliphatic content. We used the measured IE value to show that the signal at 200 u is likely to stem from species with significant aliphatic content. The measured IE at this mass lies significantly above the AIE of the $C_{16}H_8$ stabilomer (3-ethynylcyclopenta[fg]acenaphthylene). Based on recent literature, this stabilomer species appears to be a likely product of the HACA mechanism.[21, 31, 61] Hence, our PIE results at 200 u suggest that other chemical-growth mechanisms than HACA are important in this flame.

ACKNOWLEDGMENT

This work was funded by the U.S. Department of Energy (DOE), Office of Basic Energy Sciences (BES). KOJ, PE, and AV were supported by the Single Investigator Small Group Research (SISGR), Grant no. DE-SC0002619. JZ, MFC, PES, HAM, and experimental expenses, including burner design and construction, were funded under DOE BES, the Division of Chemical Sciences, Geosciences, and Biosciences. The ALS, NKRH, and KRW were supported by the Director, DOE BES, under Contract no. DE-AC02-05CH11231. Sandia National Laboratories is a multi-mission laboratory managed and operated by National Technology and Engineering Solutions of Sandia, LLC., a wholly owned subsidiary of Honeywell International, Inc., for the U.S. Department of Energy's National Nuclear Security Administration under contract DE-NA0003525.

REFERENCES

(1) Shindell, D.; Kuylenstierna, J. C.; Vignati, E.; van Dingenen, R.; Amann, M.; Klimont, Z.; Anenberg, S. C.; Muller, N.; Janssens-Maenhout, G.; Raes, F. Simultaneously Mitigating near-Term Climate Change and Improving Human Health and Food Security. *Science* **2012,** *335*, 183-189.
(2) Ramanathan, V.; Chung, C.; Kim, D.; Bettge, T.; Buja, L.; Kiehl, J.; Washington, W.; Fu, Q.; Sikka, D.; Wild, M. Atmospheric Brown Clouds: Impacts on South Asian Climate and Hydrological Cycle. *Proc. Natl. Acad. Sci. U.S.A.* **2005,** *102*, 5326-5333.
(3) Menon, S.; Hansen, J.; Nazarenko, L.; Luo, Y. Climate Effects of Black Carbon Aerosols in China and India. *Science* **2002,** *297*, 2250-2253.
(4) Ramanathan, V.; Crutzen, P.; Kiehl, J.; Rosenfeld, D. Aerosols, Climate, and the Hydrological Cycle. *science* **2001,** *294*, 2119-2124.
(5) IPCC *Climate Change 2013: The Physical Science Basis. Working Group I Contribution to the Fifth Assessment Report of the Intergovernmental Panel on Climate Change*. Cambridge University Press: Cambridge, UK and New York, NY, **2013**.
(6) Bond, T. C.; Doherty, S. J.; Fahey, D. W.; Forster, P. M.; Berntsen, T.; DeAngelo, B. J.; Flanner, M. G.; Ghan, S.; Kärcher, B.; Koch, D., et al. Bounding the Role of Black Carbon in the Climate System: A Scientific Assessment. *Journal of Geophysical Research* **2013,** *118*, 5380-5552.
(7) Finlayson-Pitts, B. J.; Pitts, J. N. Tropospheric Air Pollution: Ozone, Airborne Toxics, Polycyclic Aromatic Hydrocarbons, and Particles. *Science* **1997,** *276*, 1045-1051.

(8) Richter, H.; Howard, J. B. Formation of Polycyclic Aromatic Hydrocarbons and Their Growth to Soot—a Review of Chemical Reaction Pathways. *Prog. Energy Combust. Sci.* **2000,** *26*, 565-608.
(9) Wang, H. Formation of Nascent Soot and Other Condensed-Phase Materials in Flames. *Proc. Combust. Inst.* **2011,** *33*, 41-67.
(10) D'Anna, A. Combustion-Formed Nanoparticles. *Proc. Combust. Inst.* **2009,** *32*, 593-613.
(11) Michelsen, H. Probing Soot Formation, Chemical and Physical Evolution, and Oxidation: A Review of *in Situ* Diagnostic Techniques and Needs. *Proc. Combust. Inst.* **2017,** *36*, 717-735.
(12) Taatjes, C. A.; Hansen, N.; McIlroy, A.; Miller, J. A.; Senosiain, J. P.; Klippenstein, S. J.; Qi, F.; Sheng, L.; Zhang, Y.; Cool, T. A. Enols Are Common Intermediates in Hydrocarbon Oxidation. *Science* **2005,** *308*, 1887-1889.
(13) Cool, T. A.; McIlroy, A.; Qi, F.; Westmoreland, P. R.; Poisson, L.; Peterka, D. S.; Ahmed, M. Photoionization Mass Spectrometer for Studies of Flame Chemistry with a Synchrotron Light Source. *Rev. Sci. Instrum.* **2005,** *76*, 094102.
(14) Hansen, N.; Cool, T. A.; Westmoreland, P. R.; Kohse-Höinghaus, K. Recent Contributions of Flame-Sampling Molecular-Beam Mass Spectrometry to a Fundamental Understanding of Combustion Chemistry. *Prog. Energy Combust. Sci.* **2009,** *35*, 168-191.
(15) Li, Y.; Qi, F. Recent Applications of Synchrotron VUV Photoionization Mass Spectrometry: Insight into Combustion Chemistry. *Acc. Chem. Res.* **2009,** *43*, 68-78.
(16) Hansen, N.; Klippenstein, S. J.; Taatjes, C. A.; Miller, J. A.; Wang, J.; Cool, T. A.; Yang, B.; Yang, R.; Wei, L.; Huang, C. Identification and Chemistry of C_4H_3 and C_4H_5 Isomers in Fuel-Rich Flames. *J. Phys. Chem. A* **2006,** *110*, 3670-3678.
(17) Egolfopoulos, F. N.; Hansen, N.; Ju, Y.; Kohse-Höinghaus, K.; Law, C. K.; Qi, F. Advances and Challenges in Laminar Flame Experiments and Implications for Combustion Chemistry. *Prog. Energy Combust. Sci.* **2014,** *43*, 36-67.
(18) Moshammer, K.; Lucassen, A.; Togbé, C.; Kohse-Höinghaus, K.; Hansen, N. Formation of Oxygenated and Hydrocarbon Intermediates in Premixed Combustion of 2-Methylfuran. *Z. Phys. Chem.* **2015,** *229*, 507-528.
(19) Cao, C. The Link between the Ionization Potential and Heat of Formation for Organic Homologous Compounds. *J. Phys. Org. Chem.* **2007,** *20*, 636-642.
(20) Zhang, F.; Kaiser, R. I.; Kislov, V. V.; Mebel, A. M.; Golan, A.; Ahmed, M. A VUV Photoionization Study of the Formation of the Indene Molecule and Its Isomers. *J. Phys. Chem. Lett.* **2011,** *2*, 1731-1735.
(21) Parker, D. S.; Kaiser, R.; Bandyopadhyay, B.; Kostko, O.; Troy, T. P.; Ahmed, M. Unexpected Chemistry from the Reaction of Naphthyl and Acetylene at Combustion-Like Temperatures. *Angew. Chem.* **2015,** *127*, 5511-5514.
(22) Stein, S. E.; Fahr, A. High-Temperature Stabilities of Hydrocarbons. *J. Phys. Chem.* **1985,** *89*, 3714-3725.
(23) Frenklach, M. Reaction Mechanism of Soot Formation in Flames. *Phys. Chem. Chem. Phys.* **2002,** *4*, 2028-2037.
(24) Schuetz, C. A.; Frenklach, M. Nucleation of Soot: Molecular Dynamics Simulations of Pyrene Dimerization. *Proc. Combust. Inst.* **2002,** *29*, 2307-2314.
(25) Herdman, J. D.; Miller, J. H. Intermolecular Potential Calculations for Polynuclear Aromatic Hydrocarbon Clusters. *J. Phys. Chem. A* **2008,** *112*, 6249-6256.
(26) Elvati, P.; Violi, A. Thermodynamics of Poly-Aromatic Hydrocarbon Clustering and the Effects of Substituted Aliphatic Chains. *Proc. Combust. Inst.* **2013,** *34*, 1837-1843.

(27) Sabbah, H.; Biennier, L.; Klippenstein, S. J.; Sims, I. R.; Rowe, B. R. Exploring the Role of PAHs in the Formation of Soot: Pyrene Dimerization. *J. Phys. Chem. Lett.* **2010,** *1*, 2962-2967.
(28) Faccinetto, A.; Desgroux, P.; Ziskind, M.; Therssen, E.; Focsa, C. High-Sensitivity Detection of Polycyclic Aromatic Hydrocarbons Adsorbed onto Soot Particles Using Laser Desorption/Laser Ionization/Time-of-Flight Mass Spectrometry: An Approach to Studying the Soot Inception Process in Low-Pressure Flames. *Combust. Flame* **2011,** *158*, 227-239.
(29) Dobbins, R.; Fletcher, R. A.; Chang, H.-C. The Evolution of Soot Precursor Particles in a Diffusion Flame. *Combust. Flame* **1998,** *115*, 285-298.
(30) Skeen, S. A.; Michelsen, H. A.; Wilson, K. R.; Popolan, D. M.; Violi, A.; Hansen, N. Near-Threshold Photoionization Mass Spectra of Combustion-Generated High-Molecular-Weight Soot Precursors. *J. Aerosol Sci.* **2013,** *58*, 86-102.
(31) Johansson, K. O.; Lai, J. Y. W.; Skeen, S. A.; Popolan-Vaida, D. M.; Wilson, K. R.; Hansen, N.; Violi, A.; Michelsen, H. A. Soot Precursor Formation and Limitations of the Stabilomer Grid. *Proc. Combust. Inst.* **2015,** *35*, 1819-1826.
(32) Johansson, K. O.; Dillstrom, T.; Elvati, P.; Campbell, M. F.; Schrader, P. E.; Popolan-Vaida, D. M.; Richards-Henderson, N. K.; Wilson, K. R.; Violi, A.; Michelsen, H. A. Radical-Radical Reactions, Pyrene Nucleation, and Incipient Soot Formation in Combustion. *Proc. Combust. Inst.* **2017,** *36*, 799-806.
(33) Maricq, M. M. An Examination of Soot Composition in Premixed Hydrocarbon Flames Via Laser Ablation Particle Mass Spectrometry. *J. Aerosol Sci.* **2009,** *40*, 844-857.
(34) Öktem, B.; Tolocka, M. P.; Zhao, B.; Wang, H.; Johnston, M. V. Chemical Species Associated with the Early Stage of Soot Growth in a Laminar Premixed Ethylene–Oxygen–Argon Flame. *Combust. Flame* **2005,** *142*, 364-373.
(35) Bouvier, Y.; Mihesan, C.; Ziskind, M.; Therssen, E.; Focsa, C.; Pauwels, J. F.; Desgroux, P. Molecular Species Adsorbed on Soot Particles Issued from Low Sooting Methane and Acetylene Laminar Flames: A Laser-Based Experiment. *Proc. Combust. Inst.* **2007,** *31*, 841-849.
(36) Dobbins, R. A. Hydrocarbon Nanoparticles Formed in Flames and Diesel Engines. *Aerosol Sci. Technol.* **2007,** *41*, 485-496.
(37) Blevins, L. G.; Fletcher, R. A.; Benner, B. A.; Steel, E. B.; Mulholland, G. W. The Existence of Young Soot in the Exhaust of Inverse Diffusion Flames. *Proc. Combust. Inst.* **2002,** *29*, 2325-2333.
(38) Wornat, M. J.; Ledesma, E. B.; Sandrowitz, A. K.; Roth, M. J.; Dawsey, S. M.; Qiao, Y.-L.; Chen, W. Polycyclic Aromatic Hydrocarbons Identified in Soot Extracts from Domestic Coal-Burning Stoves of Henan Province, China. *Environmental science & technology* **2001,** *35*, 1943-1952.
(39) Wornat, M. J.; Ledesma, E. B.; Marsh, N. D. Polycyclic Aromatic Hydrocarbons from the Pyrolysis of Catechol (Ortho-Dihydroxybenzene), a Model Fuel Representative of Entities in Tobacco, Coal, and Lignin. *Fuel* **2001,** *80*, 1711-1726.
(40) Verstraete, L.; Léger, A.; d'Hendecourt, L.; Defourneau, D.; Dutuit, O. Ionization Cross-Section Measurements for Two PAH Molecules-Implications for the Heating of Diffuse Interstellar Gas. *Astron. Astrophys.* **1990,** *237*, 436-444.
(41) Li, Y. Estimated Photoionization Cross Sections, Photonionization Cross Section Database (Version 1.0). Center for Advanced Combustion & Energy (CACE): National Synchrotron Radiation Laboratory, Hefei, China, **2011**. http://flame.nsrl.ustc.edu.cn/database/ (accessed May 2016).

(42) Johansson, K. O.; Campbell, M. F.; Elvati, P.; Schrader, P. E.; Zádor, J.; Richards-Henderson, N. K.; Wilson, K. R.; Violi, A.; Michelsen, H. A. Photoionization Efficiencies of Five Polycyclic Aromatic Hydrocarbons. *submitted to J. Phys. Chem. A* **2017**.
(43) Tobita, S.; Leach, S.; Jochims, H.; Rühl, E.; Illenberger, E.; Baumgärtel, H. Single-and Double-Ionization Potentials of Polycyclic Aromatic Hydrocarbons and Fullerenes by Photon and Electron Impact. *Can. J. Phys.* **1994,** *72*, 1060-1069.
(44) Headrick, J. M.; Schrader, P. E.; Michelsen, H. A. Radial-Profile and Divergence Measurements of Combustion-Generated Soot Focused by an Aerodynamic-Lens System. *J. Aerosol Sci.* **2013,** *58*, 158-170.
(45) Zhang, X.; Smith, K. A.; Worsnop, D. R.; Jimenez, J. L.; Jayne, J. T.; Kolb, C. E.; Morris, J.; Davidovits, P. Numerical Characterization of Particle Beam Collimation: Part II Integrated Aerodynamic-Lens–Nozzle System. *Aerosol Sci. Technol.* **2004,** *38*, 619-638.
(46) Liu, P. S.; Deng, R.; Smith, K. A.; Williams, L. R.; Jayne, J. T.; Canagaratna, M. R.; Moore, K.; Onasch, T. B.; Worsnop, D. R.; Deshler, T. Transmission Efficiency of an Aerodynamic Focusing Lens System: Comparison of Model Calculations and Laboratory Measurements for the Aerodyne Aerosol Mass Spectrometer. *Aerosol Sci. Technol.* **2007,** *41*, 721-733.
(47) Johansson, K. O.; Dillstrom, T.; Monti, M.; El Gabaly, F.; Campbell, M. F.; Schrader, P. E.; Popolan-Vaida, D. M.; Richards-Henderson, N. K.; Wilson, K. R.; Violi, A. Formation and Emission of Large Furans and Oxygenated Hydrocarbons from Flames. *Proc. Natl. Acad. Sci. U.S.A.* **2016,** *113*, 8374-8379.
(48) Bohlin, A.; Kliewer, C. J. Direct Coherent Raman Temperature Imaging and Wideband Chemical Detection in a Hydrocarbon Flat Flame. *J. Phys. Chem. Lett.* **2015,** *6*, 643-649.
(49) Fierz, M.; Vernooij, M. G.; Burtscher, H. An Improved Low-Flow Thermodenuder. *J. Aerosol Sci.* **2007,** *38*, 1163-1168.
(50) Frisch, M. J.; Trucks, G. W.; Schlegel, H. B.; Scuseria, G. E.; Robb, M. A.; Cheeseman, J. R.; Scalmani, G.; Barone, V.; Mennucci, B.; Petersson, G. A., et al. *Gaussian 09*, Revision A.02; Gaussian, Inc.: Wallingford, CT, USA, **2009**.
(51) Taatjes, C. A.; Klippenstein, S. J.; Hansen, N.; Miller, J. A.; Cool, T. A.; Wang, J.; Law, M. E.; Westmoreland, P. R. Synchrotron Photoionization Measurements of Combustion Intermediates: Photoionization Efficiency and Identification of C_3H_2 Isomers. *Phys. Chem. Chem. Phys.* **2005,** *7*, 806-813.
(52) Molchanova, M. S.; Shcherbukhin, V. V.; Zefirov, N. S. Computer Generation of Molecular Structures by the Smog Program. *J. Chem. Inf. Comput. Sci.* **1996,** *36*, 888-899.
(53) Shukla, B.; Koshi, M. A Highly Efficient Growth Mechanism of Polycyclic Aromatic Hydrocarbons. *Phys. Chem. Chem. Phys.* **2010,** *12*, 2427-2437.
(54) Shukla, B.; Koshi, M. Comparative Study on the Growth Mechanisms of PAHs. *Combust. Flame* **2011,** *158*, 369-375.
(55) Hager, J. W.; Wallace, S. C. Two-Laser Photoionization Supersonic Jet Mass Spectrometry of Aromatic Molecules. *Anal. Chem.* **1988,** *60*, 5-10.
(56) Ling, Y.; Lifshitz, C. Time-Dependent Mass Spectra and Breakdown Graphs. 19. Fluoranthene. *J. Phys. Chem.* **1995,** *99*, 11074-11080.
(57) Andreocci, M.; Bicev, P.; Cauletti, C.; Piancastelli, M. The Electronic-Structure of the Pi-Systems of Acetylenic Oligomers and Related Substances-an UPS Study of Diphenylbutadiyne and Diphenylbutenyne. *Gazz. Chim. Ital.* **1980,** *110*, 31-35.

(58) Elbel, S.; Lienert, K.; Krebs, A.; tom Dieck, H. Phenylethin - Mustersonde für Substituenteneffekte. *Liebigs Ann. Chem.* **1981,** *1981*, 1785-1797.
(59) Gleiter, R.; Schäfer, W.; Eckert-Maksić, M. Transannulare Wechselwirkungen Zwischen Acetylenen–Photoelektronenspektroskopische Untersuchungen an 1, 8-Diethinylnaphthalin und Cyclischen Derivaten Von 2, 2′-Diethinylbiphenyl. *Chem. Ber.* **1981,** *114*, 2309-2321.
(60) Modelli, A.; Mussoni, L. Rapid Quantitative Prediction of Ionization Energies and Electron Affinities of Polycyclic Aromatic Hydrocarbons. *Chem. Phys.* **2007,** *332*, 367-374.
(61) Kislov, V. V.; Sadovnikov, A. I.; Mebel, A. M. Formation Mechanism of Polycyclic Aromatic Hydrocarbons Beyond the Second Aromatic Ring. *J. Phys. Chem. A* **2013,** *117*, 4794-4816.
(62) Wang, H.; Frenklach, M. A Detailed Kinetic Modeling Study of Aromatics Formation in Laminar Premixed Acetylene and Ethylene Flames. *Combust. Flame* **1997,** *110*, 173-221.

TOC Graphic

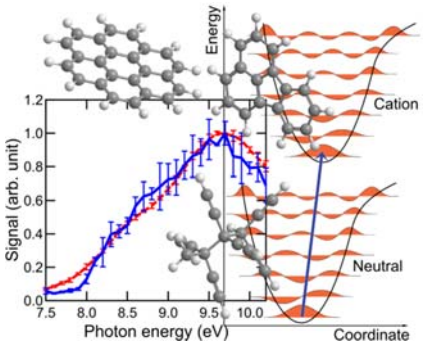
Energy
Cation
Neutral
Signal (arb. unit)
1.2
1.0
0.8
0.6
0.4
0.2
0.0
7.5
8.0
8.5
9.0
9.5
10.0
Photon energy (eV)
Coordinate